Force fields for monovalent and divalent metal cations in TIP3P water based on thermodynamic and kinetic properties

Shavkat Mamatkulov, Nadine Schwierz

Angaben zur Veröffentlichung / Publication details:

Mamatkulov, Shavkat, and Nadine Schwierz. 2018. "Force fields for monovalent and divalent metal cations in TIP3P water based on thermodynamic and kinetic properties." *The Journal of Chemical Physics* 148 (7): 074504. https://doi.org/10.1063/1.5017694.

The Journal of Chemical Physics

Force fields for monovalent and divalent metal cations in TIP3P water based on thermodynamic and kinetic properties

Cite as: J. Chem. Phys. **148**, 074504 (2018); https://doi.org/10.1063/1.5017694
Submitted: 29 November 2017 • Accepted: 31 January 2018 • Published Online: 21 February 2018

Shavkat Mamatkulov and Nadine Schwierz

Force fields for monovalent and divalent metal cations in TIP3P water based on thermodynamic and kinetic properties

Shavkat Mamatkulov[1] and Nadine Schwierz[2,a)]
[1]*Department of Physics, The Centre of Higher Technologies, Tashkent, Uzbekistan*
[2]*Department of Theoretical Biophysics, Max Planck Institute of Biophysics, 60438 Frankfurt am Main, Germany*

(Received 29 November 2017; accepted 31 January 2018; published online 21 February 2018)

Metal cations are essential in many vital processes. In order to capture the role of different cations in all-atom molecular dynamics simulations of biological processes, an accurate parametrization is crucial. Here, we develop force field parameters for the metal cations Li^+, Na^+, K^+, Cs^+, Mg^{2+}, Ca^{2+}, Sr^{2+}, and Ba^{2+} in combination with the TIP3P water model that is frequently used in biomolecular simulations. In progressing toward improved force fields, the approach presented here is an extension of previous efforts and allows us to simultaneously reproduce thermodynamic and kinetic properties of aqueous solutions. We systematically derive the parameters of the 12-6 Lennard-Jones potential which accurately reproduces the experimental solvation free energy, the activity derivative, and the characteristics of water exchange from the first hydration shell of the metal cations. In order to reproduce all experimental properties, a modification of the Lorentz-Berthelot combination rule is required for Mg^{2+}. Using a balanced set of solution properties, the optimized force field parameters aim to capture the fine differences between distinct metal cations including specific ion binding affinities and the kinetics of cation binding to biologically important anionic groups. *Published by AIP Publishing.* https://doi.org/10.1063/1.5017694

INTRODUCTION

Metal cations play an essential role in numerous physiological processes. In nature, the most abundant metal cations Na^+, K^+, Ca^{2+}, and Mg^{2+} have a significant effect on the structure, stability, and function of nucleic acids and proteins as well as in the regulation of important biomolecular processes.[1–3] Metal cations are essential since they screen the electrostatic interaction between charged biomolecules. Even more importantly, binding of metal cations to the catalytic core of metalloproteins and ribozymes allows them to execute chemical reactions that would not be possible from the basic building blocks alone.[4] Providing a quantitative description of the interaction between metal cations and biomolecules to resolve their role in transport and function is a challenging task for computer simulations.[5,6] On the one hand, *ab initio* quantum mechanical approaches could provide unbiased insight into processes involving metal cations but are limited to small systems due to high computational costs. On the other hand, classical all-atom simulations are computationally less expensive and allow us to treat larger spatial and temporal scales. However, successful molecular modeling requires accurate force fields for metal ions. Ideally, by carefully optimizing the two adjustable Lennard-Jones (LJ) parameters based on thermodynamic experimental properties, non-polarizable force fields implicitly take polarizability effects into account. At the moment, non-polarizable force fields are still more widely used and quite successful in predicting binding affinities.[7] In addition, their use can be justified further by work showing that accounting for polarizability effects is not strictly required for mono- and divalent cations since their first hydration shell is not significantly polarized compared to bulk.[8] Moreover, several recent advances in the computation of salt solubilities, activity coefficients, and chemical potentials[9–13] and advanced parameterization schemes[14] have enhanced the development of accurate models of aqueous electrolyte solutions.[15]

In the simulation of an aqueous system, the selection of the water model is the first step. Out of a large number of rigid, non-polarizable water models,[16,17] the most popular water models are the simple point charge SPC[18] or the transferable intermolecular potential TIP3P.[19] It should be noted that other water models are superior in capturing the properties of pure water.[17] Yet, the amber force fields for proteins and nucleic acids have been optimized in combination with TIP3P water explaining its widespread use in biomolecular simulations and the selection of TIP3P in our current work.

Many parameter sets for the simulation of solvated ions are available in the literature. These parameter sets are quite different since they were not chosen systematically. Rather, different optimization schemes targeting to reproduce various experimental reference data were used (see Table I and Refs. 20–22 for an overview). For instance, amber force fields formerly used amber-adapted Åqvist parameters[23] for the cations and the chloride parameters were developed by Dang.[24] The optimization of Åqvist's parameters was based on reproducing the solvation free energies. Yet, these parameters are lacking a balance between ion-water and ion-ion

a)Author to whom correspondence should be addressed: nadine.schwierz@biophys.mpg.de

TABLE I. Selected metal cation parameter sets from the literature. Amber-adapted Åqvist parameters from Ref. 23, Joung-Cheatham parameters from Ref. 22, Fyta-Netz parameters from Ref. 31, Horinek-Netz parameter set 2 (medium- -set) from Ref. 55, parameters from the standard amber database from Ref. 56, Mamatkulov-Netz parameters from Ref. 20, Allnér-Villa parameters from Ref. 50, and Li-Merz parameter set 1 (G_{solv}-set) from Ref. 32. The properties used in the optimization of the individual sets include G_{solv} (solvation free energy), S_{solv} (solvation entropy), R_1 (first maximum of the ion-water oxygen radial distribution function), LE (lattice energy), LC (lattice constant), a_{cc} (activity derivative), and (water residence time). For each set, the water model and the ion-water LJ parameters ($_{iO}$ and $_{iO}$) are listed (rounded values). The amber-adapted Åqvist parameters are obtained from the original parameters A and B via $_{ii} = (0.2/2^{1/6})$ $((2\ 762.89A/24.309B)^{1/6} - 1.768)$.

Monovalent cations			Li^+		Na^+		K^+		Cs^+	
Reference	Water	Properties	iO (nm)	iO (kJ/mol)	iO (nm)	iO (kJ/mol)	iO (nm)	iO (kJ/mol)	iO (nm)	iO (kJ/mol)
Åqvist	TIP3P	G_{solv}	0.2590	0.2207	0.3241	0.0859	0.3945	0.0295	0.4603	0.0147
Joung-Cheatham	TIP3P	G_{solv}, LE, LC	0.2488	0.2731	0.2795	0.4827	0.3094	0.7184	0.3336	1.0408
Fyta-Netz	SPC/E	G_{solv}, a_{cc}	0.2270	1.0000	0.2876	0.5160	0.2930	1.2600	0.3330	0.5000
Horinek-Netz	SPC/E	G_{solv}, S_{solv}, R_1	0.2320	0.6500	0.2700	0.6500	0.3030	0.6500	0.3300	0.6500
Current work	TIP3P	G_{solv}, a_{cc},	0.2334	0.6200	0.2879	0.2700	0.3070	0.6200	0.3350	0.6200
Divalent cations			Mg^{2+}		Ca^{2+}		Sr^{2+}		Ba^{2+}	
Åqvist	TIP3P	G_{solv}	0.2278	1.5269	0.2758	1.0946	0.3129	0.5613	0.3470	0.3542
Amber	TIP3P	G_{solv}	0.2281	1.5435	0.3102	1.1065	:::	:::	:::	:::
Mamatkulov-Netz	SPC/E	G_{solv}, a_{cc}	0.2400	0.6200	0.2790	0.7800	0.3130	0.4000	0.3500	0.2200
Allnér-Villa	mTIP3P		0.2960	0.0887	:::	:::	:::	:::	:::	:::
Li-Merz		G_{solv}	0.2719	0.1027	0.2937	0.3593	0.3065	0.5653	0.3216	0.8132
Current work	TIP3P	G_{solv}, a_{cc},	0.2385	0.6200	0.2708	1.2200	0.2987	0.8200	0.3348	0.4200

interactions leading to spontaneous crystallization at low salt concentrations and artifacts, for instance, in the simulation of DNA.[22,25] In order to overcome these shortcomings, Joung and Cheatham optimized the force fields for monovalent alkali cations based on solvation free energies, lattice energies, and inter-ionic distances of the alkali-halide crystals.[22] The Joung-Cheatham parameters for monovalent cations are now the default in amber force fields. However, for divalent metal cations, the amber-adapted Åqvist parameters are still commonly used even though they fail to reproduce thermodynamic or ion specific effects at finite concentrations.[26–28] By contrast, for Mg^{2+}, a large variety of different parameter sets exist due to its distinct role in physiological processes such as nucleic acid folding and catalytic activity (see Ref. 29 for a detailed overview over the different Mg^{2+} parameter sets). However, focusing on a single cation alone does not allow one to simulate biological processes at physiological salt composition or to identify the role of different metal cations in computer simulations of complex biological systems.

A particularly successful systematic optimization strategy has been pushed forward by Netz and co-workers for the development of ionic force fields in combination with the simple point charge-extended (SPC/E) water model.[20,21,30,31] Their optimization is based on single-ion and ion-pair properties and allows them to simultaneously reproduce several thermodynamic properties of an ionic solution at finite concentrations. In progressing toward improved force fields, the aim of our current work is to simultaneously reproduce thermodynamic and kinetic properties of aqueous salt solutions. The approach presented here is an extension of previous efforts with the aim to provide improved force fields for the metal cations Li^+, Na^+, K^+, Cs^+, Mg^{2+}, Ca^{2+}, Sr^{2+}, and Ba^{2+} for biomolecular simulations in combination with the TIP3P water model. We systematically derive the parameters to reproduce the experimental solvation free energies, the activity derivatives, and the characteristics of water exchange from the first hydration shell. Targeting these experimental properties, the force field is expected to correctly capture the following quantities in the best possible way: (i) ion-water interactions in particular ion hydration, (ii) ion-paring properties which are integral to quantify cation binding affinities to anionic biological groups, and (iii) the characteristics of water exchange which is important for cation binding kinetics.

Our optimization procedure is done in three consecutive steps: In the first step, the ion-water interactions are optimized by selecting combinations of LJ parameters that reproduce the experimental solvation free energy. The first peak in the ion-water radial distribution function (rdf) and the number of water molecules in the first hydration shell are used to gain further insight into the structural properties of single ions in water. In the second step, we optimize the ion-ion interactions by selecting parameter combination that simultaneously match experimental activity derivatives. For Mg^{2+}, simultaneous matching of single-ion and ion-pair properties is only possible by rescaling the effective cation-anion radius, using a modification of the standard Lorentz-Berthelot combination rule similar as in Ref. 20. For Ca^{2+} and Sr^{2+}, we find degenerate parameter sets that describe the experimental data equally well. Therefore, in the last step of our optimization, we account for the kinetics of water exchange from the first hydration shell of the metal cations. For the monovalent cations, the experimental trends are reproduced without any further adjustments, while for the divalent cations, experimental water exchange rates unambiguously determine the final set.

METHODS

Molecular dynamics (MD) simulations

The most common form of the pairwise potential is the LJ potential with a repulsive r^{-12} and an attractive r^{-6} term. Other potential forms have been introduced in the literature.[29,32] Yet, our motivation to use 12-6 potentials are their simple form, computational efficiency, and transferability. Here, the pair interaction potentials U_{ij} has the following form:

$$U_{ij}(r_{ij}) = \frac{q_i q_j}{4\pi\epsilon_0 r_{ij}} + 4\varepsilon_{ij}\left[\left(\frac{\sigma_{ij}}{r_{ij}}\right)^{12} \quad \left(\frac{\sigma_{ij}}{r_{ij}}\right)^{6}\right], \qquad (1)$$

where q_i, q_j are the charges of the atoms i, j and r_{ij} is the distance between these atoms. The Coulomb term is free from adjustable parameters while the LJ parameters ε_{ij}, the LJ interaction strength, and σ_{ij}, the corresponding LJ diameter, are free to be optimized to reproduce certain physical properties as discussed in the following. In addition, we use the Lorentz-Berthelot combination rules

$$\varepsilon_{ij} = \sqrt{\varepsilon_i \varepsilon_j}; \qquad \sigma_{ij} = \frac{\sigma_i + \sigma_j}{2}, \qquad (2)$$

where i, j correspond to the index of the ions. We employ the TIP3P water model. The TIP3P water model assigns partial charges of −0.834 and 0.417 to oxygen and hydrogen and LJ parameters of $\sigma_{OW} = 3.150\,61$ Å and $\varepsilon_{OW} = 0.6364$ kJ/mol.[19] The geometry is fixed at a bond length of 0.9572 Å and a bond angle of 104.52 using the SHAKE algorithm.

All simulations are performed using GROMACS 5.1.2 with periodic boundary conditions in all three directions and particle mesh Ewald summation with tin foil boundary conditions and a Fourier spacing of 0.12 nm and a grid interpolation up to order 4 to handle long-range electrostatic forces and the electroneutrality condition. Close Coulomb real space interactions are cut off at 1.2 nm and LJ interactions are cut off after 1.2 nm, respectively. Long-range dispersion corrections for energy and pressure are applied to account for errors stemming from truncated LJ interactions.

Initial energy minimization is performed with the steepest descent algorithm. For each free energy perturbation (FEP) or continuous simulation, a NVT and a NPT equilibration is done for 1 ns, controlling the temperature at 300 K with the Berendsen thermostat and the pressure at 1 bar with the Berendsen barostat. During NVT and NPT equilibration, we apply position restraints to all ions in the simulation box to avoid ion-pair formation before an appropriate hydration shell has been developed. All production runs are performed at a temperature of 300 K using the velocity rescaling thermostat, a pressure of 1 bar using the Parrinello Rahman barostat, and a time step of 2 fs. All parameters used in the MD simulations have been previously checked to lead to consistent results for the systems under study.[30,31]

Free energy perturbation simulations

The solvation free energies of the ions are calculated using free energy perturbation (FEP) simulations, evaluated with the Bennett acceptance ratio (FEP/BAR) method. The simulations are performed by placing a single ion in a cubic simulation box cubic box (L = 25 Å) and adding 506 TIP3P water molecules. The production run is done for 1 ns discarding the first 200 ps for equilibration. The solvation pathway is split into two separate processes: first, a neutral LJ particle is created, then the charge is increased in a second step. Along the solvation pathway, a transformation parameter λ is used with 20 evenly spaced replicas for applying the LJ interaction potential. For the Coulomb potential, 10 replicas are used for the monovalent cations and 20 replicas are used for the divalent cations. To improve convergence, soft-core potentials are applied for LJ potentials with $\alpha = 0.3$, linear lambda scaling, and a radius power of 6.

Self-diffusion coefficient of a single ion in water

For the final set of LJ parameters, the self-diffusion coefficient is calculated from an additional 50 ns NVT simulation of the single ions using 3 different sizes of the cubic simulation box (L = 25 Å, L = 30 Å, L = 35 Å). The NVT ensemble is chosen since the results are expected to be very close to the NVE ensemble in which diffusion coefficients should be calculated ideally.[29] All simulations are pre-equilibrated in the NPT ensemble before fixing the box size. Self-diffusion coefficients are calculated from the slope of the mean-square displacement. After a brief initial period of about 1 ps, the mean-square displacement grows linearly and the diffusion coefficient is estimated from a straight line fit. The diffusion coefficient corrected for system size effects reads[33]

$$D_0 = D_{\mathrm{pbc}}(L) + \frac{k_B T \xi_{ew} \alpha}{6\pi\eta L}, \qquad (3)$$

where L is the box length, D_{pbc} is the computed self-diffusion coefficient, D_0 is the diffusion coefficient for infinite non-periodic systems, k_B is the Boltzmann constant, T is the absolute temperature, η is the solvent viscosity, and $\xi_{ew} = 2.837\,297$ is the self-term for a cubic lattice. The empirical parameter α accounts for deviations from the Oseen point-particle limit. In the following, we use $\alpha = 1.0$ for all cations. To correct for the low viscosity of TIP3P water compared to the measured water viscosity, we report the scaled diffusion coefficients,

$$D = \frac{\eta_{\mathrm{tip3p}}}{\eta_{\mathrm{water}}} D_0 \qquad (4)$$

with the viscosity of TIP3P water $\eta_{\mathrm{tip3p}} = 3.13 \quad 10^{-4}$ kg m^{-1} s^{-1} and the experimentally measured water viscosity $\eta_{\mathrm{water}} = 8.91 \quad 10^{-4}$ kg m^{-1} s^{-1}.[17] Errors of the self-diffusion coefficient correspond to the standard deviation of the three independent simulations with different box sizes.

Finite concentration simulations

The initial configurations of the electrolyte solutions are generated from a cubic box (L = 40 Å) of 2180 TIP3P water molecules by randomly replacing water by ions until the required concentration is attained. After the replacements, there are 19 divalent cations or 38 monovalent cations and 38 anions in the box, corresponding to a molality of about 0.5M or 1M. A few simulations are performed at higher concentrations. The simulations are done for 150 ns and trajectories are recorded every 0.2 ps to gather better statistics. The radial

distribution functions (rdfs) of the salt solutions are obtained using GROMACS, neglecting the first 1 ns for equilibration. The number of water molecules in the first hydration shell is calculated by counting the water molecules within a cutoff distance r_{cut} defined by the first minimum in the ion-water radial distribution function. Specifically, the following values for r_{cut} were used: 0.3 nm (Mg^{2+}), 0.33 nm (Ca^{2+}), 0.34 nm (Sr^{2+}), 0.36 nm (Ba^{2+}), 0.28 nm (Li^{+}), 0.32 nm (Na^{+}), 0.35 nm (K^{+}), 0.387 nm (Cs^{+}).

Water residence time and free energy profiles (PMFs)

The mean lifetime of the water molecules in the first hydration shell around the metal cations with the exception of Mg^{2+} is calculated directly by following the motion of all water molecules. The average lifetime is obtained by averaging the times that water molecules remain within the cutoff distance defined above. The free energy profiles (PMFs) are obtained from the ion-water oxygen rdf from Boltzmann inversion. For Mg^{2+}, the water residence time is on the order of a microsecond[34] and therefore cannot be obtained in a straightforward MD simulation with sufficient statistics. Instead, the PMF is calculated from umbrella sampling. For ion-water distances between 0.2 and 0.6 nm, we use a force constant $k = 100\,000$ kJ/(mol nm^2) and a window spacing of 0.01 nm. For larger distances between 0.5 and 1 nm, we use $k = 1000$ kJ/(mol nm^2) and a window spacing of 0.02 nm. The umbrella simulations are performed for 10 ns discarding 500 ps for equilibration. The PMF is calculated using the weighted histogram analysis method,[35] and a Jacobian correction is applied to reconstruct the true PMF since we are using distances rather than Cartesian coordinates,[36]

$$\mathrm{PMF}(r) = \mathrm{PMF}_{\mathrm{WHAM}}(r) + 2k_{\mathrm{B}}T\ln(r). \tag{5}$$

Solvation free energy and correction terms

The ionic solvation free energy calculated from simulations is sensitive to the simulation scheme and treatment of the electrostatic forces. Therefore, for comparison with experimental data, several corrections have to be applied to the raw simulation data. The correction term accounting for finite size effects[37] for an ion with valency z reads

$$G_{fs} = \frac{z^2 N_A e^2}{4\pi\varepsilon_0}\Big[\ \frac{\xi_{e\mathrm{w}}}{2\varepsilon_r L} + \Big(1\ -\ \frac{1}{\varepsilon_r}\Big)\Big(\frac{2\pi R_1^2}{3L^3}\ -\ \frac{8\pi^2 R_1^5}{45L^6}\Big)\Big], \tag{6}$$

where N_A is Avogadro's number, e is the unit charge, R_1 is the effective radius of the ion, estimated as the first peak in the ion-oxygen rdf, and $\varepsilon_r = 83$ is the relative dielectric constant of the TIP3P water.[38] The Wigner potential is $\xi_{e\mathrm{w}} = -2.837\,279/L$, where L is the simulation box size in nm.[39,40] Experimental values of the solvation free energies are usually given with respect to a hypothetical transfer of ions from the ideal gas phase of $p_0 = 1$ atm pressure to the ideal solution under pressure of $p_1 = 24.6$ atm, corresponding to the density of 1 mol/l. Thus, it is also necessary to include a correction term related to the compression of the gas

$$G_{press} = N_A k_B T \ln(p_1/p_0) = 7.9\ \text{kJ/mol}, \tag{7}$$

where $k_B T$ is the thermal energy. In the experiments, the ions have to pass the air-water interface in order to enter into the aqueous phase. The corresponding free energy correction term is

$$G_{surf} = N_A z\quad e\phi_{surf} =\quad z\quad 50.8\ \text{kJ/mol}, \tag{8}$$

where we choose the surface potential as $\phi_{surf} = -0.527$ V.[41] Hence, the total single-ion solvation free energy is given by

$$G_{\mathrm{solv}} =\quad G_{sim} +\quad G_{fs} +\quad G_{surf} +\quad G_{press}. \tag{9}$$

Extracting single-ion solvation free energies from experimental data usually relies on the solvation free energy of the proton $G_{\mathrm{solv}}(H^+)$. However, the proton solvation free energy is perturbed by the surface potential of water, which is not exactly known and prone to errors. A popular estimate for $G_{\mathrm{solv}}(H^+)$ is that of Tissandier *et al.*[42] (−1104.5 kJ/mol). This value is 50 kJ/mol lower than the other commonly used value of Marcus[43] (−1056 kJ/mol).

Experimental solvation free energy data are more robust for neutral ion-pairs, for which the water surface potential drops out. Therefore, we use experimental data for neutral ion-pairs in our optimization. As a reference ion, we choose the chloride ion. As a starting point, we choose the Dang-Smith parameters for Cl^- using $\sigma_{\mathrm{iO}} = 3.78$ Å and $\varepsilon_{\mathrm{iO}} = 0.52$ kJ/mol.[44] The Smith-Dang parameters were optimized for the SPC/E water model and give a solvation free energy of $G_{\mathrm{solv}} = -306$ kJ/mol,[21] close to the absolute solvation free energy of Cl^- based on Tissandier's estimate. The LJ parameter $\varepsilon_{\mathrm{iO}}$ is then modified in TIP3P water until it reproduces the absolute solvation energy, given by $G_{\mathrm{solv}} = -304.2$ kJ/mol[42] (see Fig. 1). The resulting LJ parameters are listed in Table II.

For the divalent cations, the solvation free energies are always the sum of the cationic and the chloride free energy, respectively,

$$_G =\quad G_{\mathrm{solv}} + z\qquad G_{\mathrm{solv}}(Cl\ ), \tag{10}$$

where z is the valency of the cation. For the divalent cations, we sample the LJ parameters σ_{iO} and ε_{iO} on a 21 7 grid. The range $\sigma_{iO} = 2.2 - 4.25$ Å and $\varepsilon_{iO} = 0.02 - 1.28$ kJ/mol is studied. For an efficient optimization of σ_{iO} and ε_{iO}, the surface of the solvation free energy is fitted as linear interpolation between σ_{iO} values for constant ε_{iO}.

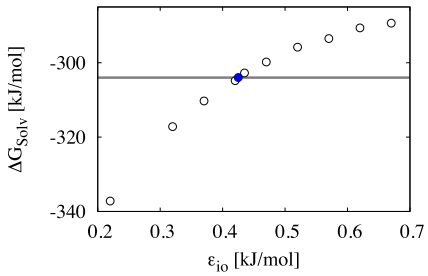

FIG. 1. Solvation free energy of the reference chloride ion in TIP3P water. Starting from the Dang-Smith parameters[44] commonly used in combination with the SPC/E water model, the LJ parameter " $_{\mathrm{iO}}$ is modified. The horizontal line is the experimental solvation free energy from Ref. 43 using Tissandier's estimate for the proton solvation free energy.[42] The filled symbol denotes the optimized parameter for chloride.

TABLE II. Optimized force field parameters for Cl^- for simulations with the TIP3P water model. The ion-water and ion-ion LJ parameters ($_{iO}$, $_{iO}$, $_{ii}$, and $_{ii}$), the solvation free energy G_{solv} from simulations with the final parameter set and experiments[43] using Tissandier's estimate for the proton solvation free energy,[42] and R_1 are listed. The experimental value R_1^{exp} is taken from the data collection from Ref. 57.

	$_{iO}$ (nm)	$_{iO}$ (kJ/mol)	$_{ii}$ (nm)	$_{ii}$ (kJ/mol)	G_{solv} (kJ/mol)		G_{solv}^{exp} (kJ/mol)	R_1 (nm)		R_1^{exp} (nm)	
Cl^-	0.378	0.425	0.441	0.284	−303.9	0.5	−304.2	0.319	0.001	0.319	0.007

Kirkwood-Buff (KB) theory

We use Kirkwood-Buff (KB) theory to obtain the activity derivatives of the salt solutions, as was done before in similar studies.[45] The KB theory connects integrals over pair distribution functions to thermodynamic quantities such as isothermal compressibilities, partial molar volumes, and in particular solution activity derivatives. The KB integrals are defined as[27]

$$G_{ij} = 4\pi \int_0^1 (g_{ij}^{VT}(r) \quad 1) r^2 dr, \tag{11}$$

where $g_{ij}^{VT}(r)$ is the rdf between species i and j in the grand canonical ensemble. The KB integrals are defined for systems open to all solution components. However, since most simulations are performed in closed systems, the KB integrals are commonly approximated by truncating the integral after a certain distance

$$G_{ij} \quad 4\pi \int_0^R (g_{ij}^{NpT}(r) \quad 1) r^2 dr, \tag{12}$$

where R represents the correlation distance in which the solution composition deviates from bulk. This approximation has been shown to be valid for large systems ($L > 4$ nm) and sufficient sampling (>5 ns).[46] With the KB integrals, we can compute the derivative of the activity coefficients, a_{cc}, of electrolyte solutions as follows:

$$a_{cc} = \left(\frac{\partial \ln a_c}{\partial \ln \rho_c}\right)_{|p,T} = 1 + \left(\frac{\partial \ln y_c}{\partial \ln \rho_c}\right)_{|p,T} = \frac{1}{1 + \rho_c(G_{cc} \quad G_{cw})}, \tag{13}$$

where the molar activity coefficient y_c is defined via $a_c = \rho_c y_c$, while ρ_c is the cosolvent number density and a_c is the activity. For monovalent ions, these equations take the following forms:[46]

$$G_{cc}^{(1)} = \frac{1}{4}[G_{++} + G \quad + 2G_{+} \ ] \tag{14}$$

and

$$G_{cw}^{(1)} = G_{wc}^{(1)} = \frac{1}{2}(G_{+w} + G \ _{w}), \tag{15}$$

as given in Refs. 31 and 45. The expressions for the divalent ions are

$$G_{cc}^{(2)} = \frac{1}{9}[G_{++} + 4(G \quad + G_{+} \ )], \tag{16}$$

$$G_{cw}^{(2)} = G_{wc}^{(2)} = \frac{1}{3}G_{+w} + \frac{2}{3}G \ _{w}. \tag{17}$$

Errors of the activity derivatives are estimated through block averaging of the MD data with a total time of 150 ns in blocks of 45 ns duration. The rdfs are directly obtained from the MD simulation trajectories as discussed earlier. In order to achieve accurate results, finite size effects need to be taken into account. Of particular importance is the condition that the rdf reaches unity at large distances. We introduce a correcting factor such that the rdf used in the calculations of the KB integrals is written as $g_{ij}(r^0\rho) = f(\rho)g_{ij}^{sim}(r)$ with a prefactor $f(\rho)$ that is adjusted to ensure the correct asymptotic behavior at large distances.[47] Note that the convergence of the usual KB integrals used here can be improved by extrapolating exact expressions for volume centered integrals.[48,49]

RESULTS AND DISCUSSION

In the following, we present the results of our optimization procedure. The optimization is done in three consecutive steps and is designed to simultaneously reproduce the experimental solvation free energy, ion-pairing properties measured by activity derivatives, and water exchange kinetics of cations in aqueous solutions. The optimized parameters are given in Tables II and III. A comparison of all properties calculated with the optimized parameters and experimental reference data is given in Tables IV and V including solvation free energies, coordination numbers, positions of the first maximum of the ion-water oxygen radial distribution function, activity derivatives, water residence times in the first hydration shell, and self-diffusion coefficients.

Solvation free energy

The solvation of the monovalent and divalent cations is a very favorable process with a free energy gain of several hundred kJ/mol. Figure 2 shows the simulation results for the solvation free energy, G_{solv}, as a function of the LJ

TABLE III. Optimized force field parameters for monovalent and divalent metal cations for simulations with the TIP3P water model. The ion-water and ion-ion LJ parameters ($_{iO}$, $_{iO}$, $_{ii}$, and $_{ii}$) are listed. The results for the final parameter set for all single-ion, ion-pair, and kinetic properties are shown in Tables IV and V.

	$_{iO}$ (nm)	$_{iO}$ (kJ/mol)	$_{ii}$ (nm)	$_{ii}$ (kJ/mol)
Li^+	0.233 437	0.62	0.151 813	0.604 036
Na^+	0.287 89	0.27	0.260 719	0.114 553
K^+	0.306 95	0.62	0.298 839	0.604 036
Cs^+	0.334 988	0.62	0.354 915	0.604 036
Mg^{2+}	0.238 50	0.62	0.161 939	0.604 036
Ca^{2+}	0.270 773	1.22	0.226 453	2.338 83
Sr^{2+}	0.298 723	0.82	0.282 385	1.056 59
Ba^{2+}	0.334 838	0.42	0.354 615	0.277 19

TABLE IV. Results for single-ion properties for the optimized parameters in direct comparison with experimental results. Solvation free energy of neutral cation-chloride pairs $_G$, maximum of the ion-water oxygen rdf R_1, and coordination number n_1 from simulations for 1M (monovalent cations) or 0.5M (divalent cations) salt concentration.

Ion	$_G$ (kJ/mol)	$^{\text{exp}}_{G}$ [a] (kJ/mol)	n_1	n_1^{exp} [b]	R_1 (nm)	R_1^{exp} [b] (nm)
Li^+	−826.6	−828	4.19 0.02	4-6 (4)	0.197 0.001	0.208 0.006
Na^+	−720.7	−722	5.53 0.02	4-8 (6)	0.233 0.001	0.236 0.006
K^+	−649.2	−651	6.49 0.01	6-8	0.267 0.001	0.280 0.008
Cs^+	−603.5	−605	7.77 0.01	7-8	0.297 0.001	0.314 0.008
Mg^{2+}	−2531.1	−2532	6	6	0.195 0.001	0.209 0.004
Ca^{2+}	−2208.9	−2209	7.79 0.01	8[c]	0.238 0.001	0.242 0.005
Sr^{2+}	−2079.7	−2080	8.11 0.01	7.9-8	0.252 0.001	0.264 0.004
Ba^{2+}	−1951.7	−1952	8.57 0.06	9[d]	0.277 0.001	0.290 0.006

[a]Experimental values are from Ref. 43.
[b]Experimental values are from Ref. 57.
[c]Experimental values are from Ref. 58.
[d]Experimental values are from Ref. 59.

parameters σ_{iO} and ε_{iO}. The statistical error of the simulated solvation free energy is about 1 kJ/mol. The variation of G_{solv} with ε_{iO} is less pronounced while the charge density and therefore the effective cation size σ_{iO} has a significant influence: The higher the charge density, i.e., the smaller the σ_{iO}, the more the favorable the solvation is. Similarly, G_{solv} is much more negative for divalent cations compared to monovalent cations with the same effective size. From the grid shown in Fig. 2, the solvation free energy isolines are constructed by selecting σ_{iO}-ε_{iO} combinations that reproduce the experimental solvation free energy $_G$ with chloride as the counterion. In the following, all properties of the metal cations are presented as a function of these σ_{iO}-ε_{iO} combinations.

The free energy isolines for all mono- and divalent cations are shown in Fig. 3 in direct comparison with parameter sets from the literature (see Table I). Force field parameters that have been optimized to match the solvation free energy are close to the same isoline indicating a minor influence of the water model. The Åqvist parameters developed in 1990 slightly underestimate the solvation free energy. This deviation simply reflects that simulation protocols have improved, especially the treatment of long-ranged electrostatic interactions employing the particle mesh Ewald treatment, leading to more accurate calculations. On the other hand, models that target properties other than the G_{solv}, including cation-water distances, coordination numbers, or water exchange free energy barriers largely underestimate G_{solv} (for instance, by 84.4 kJ/mol for Mg^{2+} with mTIP3P by Allnér[50] or by 220 kJ/mol for Ca^{2+} with TIP3P and the standard amber parameters[51]). These deviations reflect the challenge of reproducing experimental structural, thermodynamic, and kinetic properties simultaneously using simple 12-6 potentials.

To provide insight into important ion-water structural properties, we calculate the number of water molecules in the first hydration shell, n_1, and the first peak in the ion-water radial distribution function, R_1, along the free energy isolines (Fig. 4). n_1 is well captured along the free energy isolines for all cations [Fig. 4(a)]. On the other hand, it is obvious from Fig. 4(b) that the experimental values for R_1 (horizontal gray bars) are not exactly reproduced for any parameter combination. It has been observed previously that simultaneously reproducing G_{solv} and R_1 is not possible using simple 12-6

TABLE V. Results for ion-pairing and kinetic properties for the optimized parameters in direct comparison with experimental results. Activity derivative a_{cc} from simulations and experiments[52] for 1M (monovalent cations) or 0.5M (divalent cations) salt concentration. Residence time of water in the first hydration shell from simulations with the same salt concentration and experiments.[34] Self-diffusion coefficient D at infinite dilution from simulations and experiments.[43]

Ion	a_{cc}	a_{cc}^{exp}	(ps)	$^{\text{exp}}$ (ps)	D (10^5 cm^2/s)	D^{exp} (10^5 cm^2/s)
Li^+	1.08 0.04	1.143	39.9 0.4	<100	1.07 0.04	1.029
Na^+	0.99 0.06	0.974	25.3 0.1	<100	0.96 0.17	1.334
K^+	0.88 0.05	0.902	9.4 0.02	<100	1.48 0.11	1.957
Cs^+	0.87 0.03	0.846	6.3 0.01	<100	1.45 0.05	2.056
Mg^{2+}	1.03 0.05	1.083	:::	1.49 10^6	0.71 0.05	0.706
Ca^{2+}	0.99 0.03	1.028	187.3 3.8	<100	0.69 0.031	0.791
Sr^{2+}	1.05 0.02	0.989	181.6 3.2	<100	0.66 0.03	0.792
Ba^{2+}	0.95 0.06	0.913	147.7 4.5	<100	0.64 0.03	0.847

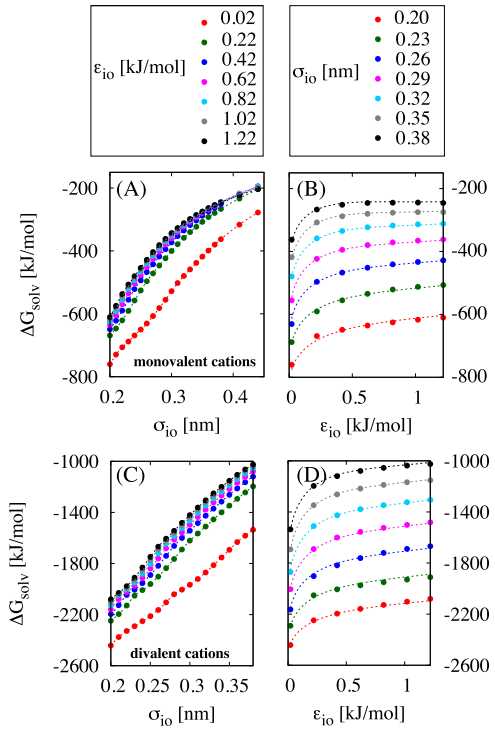

FIG. 2. Solvation free energy G_{solv} of monovalent (top) and divalent metal cations (bottom) as a function of the LJ parameter $_{iO}$ [(a) and (c)] and "$_{iO}$ [(b) and (d)]. Symbols show the points obtained from simulations. Lines represent cuts of the fitted free energy surface.

potentials.[21,51] Other potential forms with additional parameters such as 12-6-4 potentials[32] might perform better in this respect but are outside the scope of our present work.

In the further parameter design, we have to make a compromise: As the most important single-ion property, we choose to exactly reproduce the solvation free energy at the expense of underestimating the cation-oxygen distance. The first optimization step determines all possible σ_{iO}-ε_{iO} combinations. Since other single-ion properties including R_1 and n_1 are correlated, they do now allow us an unambiguous parameter determination. Therefore, our next optimization step is based ion-pairing properties at finite salt concentrations.

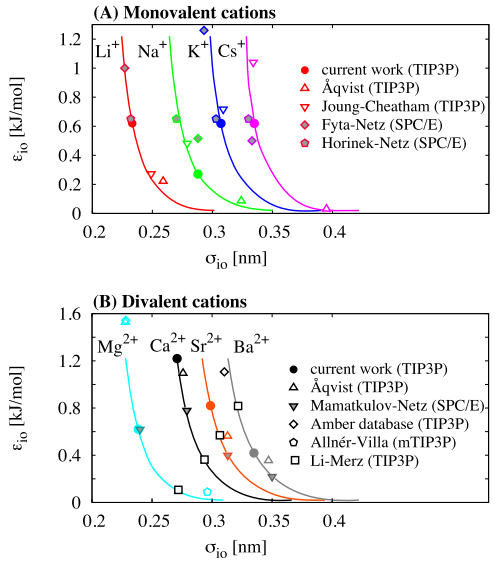

FIG. 3. Combinations of $_{iO}$ and "$_{iO}$ that reproduce the experimental solvation free energies (solid lines) for monovalent (a) and divalent cations (b). Open symbols correspond to parameter sets from the literature that were optimized in combination with the TIP3P water model. Grayed out symbols correspond to parameter sets optimized with the SPC/E water model. Filled circles indicate our final choice of parameters. All values are listed in Tables I and III.

Activity derivatives of electrolytes

In the following, we aim to select the parameter combinations that capture ion-pairing properties, i.e., parameters that provide a proper balance between ion-water and ion-ion interactions. Insight into ion-pairing properties is obtained from experimental activity coefficients which measure the deviation from ideal behavior. In an ideal solution of non-interacting particles, the activity coefficient is one and deviations indicate ion-ion and ion-solvent interactions. Hence, the activity coefficient is sensitive to ion-pairing properties of electrolyte solutions.

In our optimization procedure, we calculate the activity derivative of the activity coefficient with respect to the concentration from the Kirkwood-Buff theory [Eq. (13)]. The activity derivative can be compared readily to the abundant experimental data.[52] Figure 5 shows the results for the activity derivative for the monovalent and the divalent cations with chloride as the counterion in comparison to the experimental results (horizontal gray bars from Ref. 52). The experimental activity derivative increases with increasing charge density of the cations. The reason for this trend is the following: In an electrolyte solution composed of ions with similar charge density, such as CsCl, the ion-ion affinity is larger compared to the ion-water affinity. Therefore, these ions spontaneously form inner-sphere ion-pairs and the activity derivative is smaller than one. By contrast, for ions with dissimilar charge density, such as LiCl, the ion-water interaction is much stronger than the ion-ion interaction. Consequently, the ions prefer to remain solvent separated and the activity derivative is larger than one. Even more importantly, the same trend is observed when going along the free energy isoline (open points in Fig. 5). For each cation, the activity derivative increases from left (large σ_{iO}, large ion-pairing probability) to right (small σ_{iO}, small ion-pairing probability). For the monovalent cations, the optimal σ_{iO}-ε_{iO} combination is uniquely determined by the intersection point with the experimental data.

The situation is more complex for the divalent cations for two reasons: (i) For $MgCl_2$, the parameter optimization problem is overdetermined, i.e., there are no combinations of LJ parameters that allow us to simultaneously match the solvation free energy and the activity derivative. (ii) For $CaCl_2$ and $SrCl_2$, the optimization problem is underdetermined, i.e., there are several sets of parameter combinations that perform equally well at matching the solvation free energy and the activity derivative. In the following, we show how to solve both problems (i) by going beyond standard combination rules and (ii) by taking the kinetics of water exchange from the first hydration shell into account.

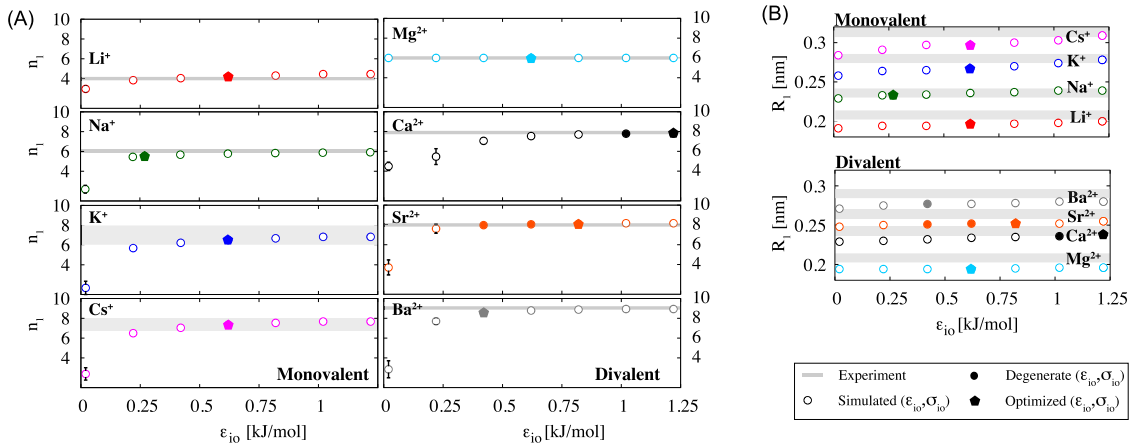

FIG. 4. Structural properties of the cations using ε_{iO}-σ_{iO} combinations from the free energy isolines: (a) Number of water molecules in the first hydration shell n_1 of the cations as a function of the ion-water LJ parameter ε_{iO} on the isoline shown in Fig. 3. (b) Position of the first peak in the ion-water oxygen rdf R_1 as a function of the ion-water LJ parameter ε_{iO} on the free energy isoline for the monovalent ions (top) and the divalent cations (bottom). Horizontal lines denote the respective experimental results with the line width indicating the experimental uncertainty (Table IV). Symbols correspond to the simulated values, and filled symbols are degenerate parameter sets that simultaneously reproduce the experimental solvation free energy and the activity derivative. The filled diamonds denote the optimized parameter set.

Beyond standard mixing rules for Mg^{2+}

As discussed in the section titled Activity derivatives of electrolytes, it is not possible to simultaneously match the solvation free energy and the activity derivative for Mg^{2+} (Fig. 5). To overcome this problem, we follow the previously proposed scheme that modifies the standard Lorentz-Berthelot combination rule for the effective anion-cation radius[31] by using a freely adjustable parameter λ ,

$$\sigma_{+-} = \lambda \frac{\sigma_{+} + \sigma_{-}}{2}. \tag{18}$$

With this approach, the solvation free energy remains unchanged since the ion-water interactions are not affected. Changing the effective anion-cation radius has the following effect on the cation-anion radial distribution function $g_{+-}(r)$ shown in Fig. 6(a): With increasing λ , the first peak in $g_{+-}(r)$ corresponds to the solvent-shared ion-pair decreases. Note that for $MgCl_2$ no inner-sphere contact pairs occur due to the mismatching charge density of the ions. Still, with increasing λ , the probability of forming solvent-shared ion-pairs decreases and consequently the activity derivative increases.

In order to select the correct value for λ , we perform simulations at three different salt concentrations (0.5M, 1M, and 2M). From these simulations, we selected the value that reproduces the experimental data for the different concentrations [Fig. 6(b)]. Finally, using λ = 1.65 allows us to capture the activity derivative over a broad concentration range [Fig. 6(c)]. In order to further validate our newly developed force field parameters, we performed simulations for all metal cations for larger salt concentration and achieved very good agreement with experimental data up to 2M concentrations (Figs. S1 and S2 in the supplementary material).

Water exchange from the first hydration shell

In the following, we focus on the water molecules in the first hydration shell of the mono- and divalent metal cations and calculate their mean residence time. For all ions with the exception of Mg^{2+}, water exchange times are on the order of a

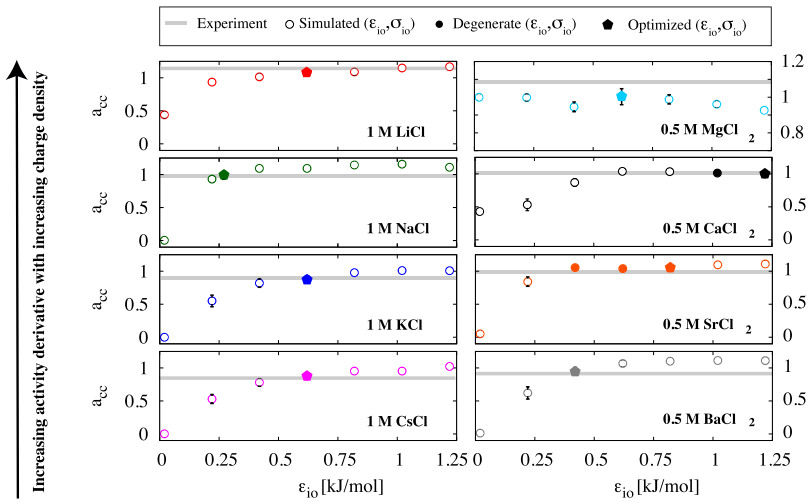

FIG. 5. Activity derivatives for 1M LiCl, NaCl, KCl, and CsCl (left) and 0.5M $MgCl_2$, $CaCl_2$, $SrCl_2$, and $BaCl_2$ (right) as a function of the ion-water LJ parameter ε_{iO} on the free energy isoline. Open symbols correspond to the simulated values with ε_{iO}-σ_{iO} combinations from the free energy isolines. Horizontal lines denote the respective experimental results at the same concentration (Table V). Filled symbols are degenerate parameter sets that reproduce experimental solvation and ion-pairing properties. Filled diamonds denote the optimized parameter set.

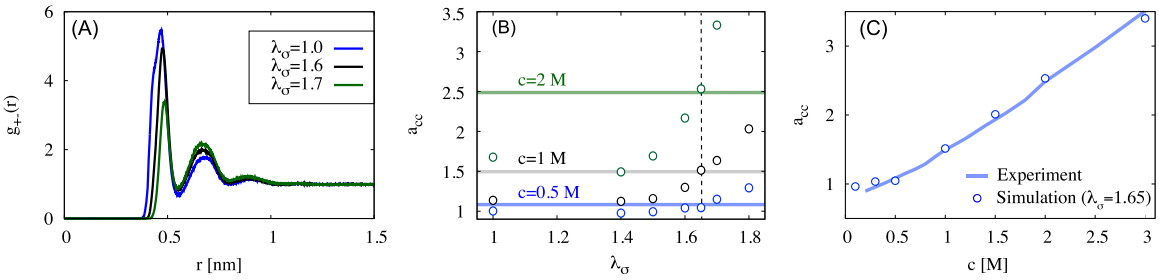

FIG. 6. Modification of the standard mixing rule: (a) Radial distribution function $g_{+-}(r)$ for Mg^{2+} and Cl^- for different values of the scaling parameter σ. (b) Activity derivative for $MgCl_2$ for different concentrations as a function of σ. The horizontal lines correspond to the respective experimental results at the same concentration. The dashed vertical line indicates the optimal values σ = 1.65 for matching the experimental values. (c) Activity derivative as a function of the salt concentration from simulations with σ = 1.65 (open points) and experimental results from Ref. 52 (line).

few hundred picoseconds and can be calculated from a straightforward MD simulation (see the section titled Methods). In experiments, the time resolution is insufficient to measure the lifetime of the water molecules for these fast exchanges which has been estimated to be smaller than 100 ps.[34] Still, insight into the kinetics can be obtained from ligand exchange experiments.[34]

Figures 7(a) and 8(a) show the mean lifetime τ, i.e., the time a water molecule remains on average in the first hydration shell as a function of ε_{iO} for the monovalent and divalent metal cations. For the monovalent cations, τ decreases with increasing ε_{iO} [Fig. 7(a)]. The reason for this decrease is that by increasing ε_{iO} the ion-water LJ interaction becomes more attractive leading to a reduction of the free energy barrier associated with water exchange. The free energy profile (PMF) underlying the removal of one water molecule from the first hydration shell as a function of the ion-water oxygen distance is shown in Fig. 7(b) for the optimal parameter set. For the monovalent ions, the optimal LJ parameters are already uniquely determined based on the solvation free energy and the activity derivative. Without any further optimization, the results are in agreement with the general trends expected from

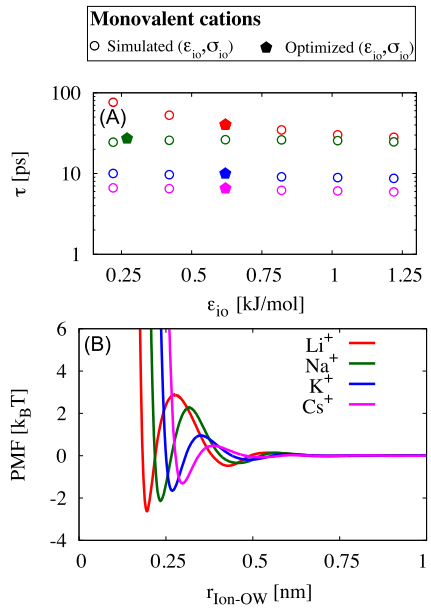

FIG. 7. Water exchange in the first hydration shell of monovalent metal cations: (a) Average lifetime of the water molecules in the first hydration shell of the cations as a function of the ion-water LJ parameter ε_{iO} on the free energy isoline for 1M salt concentration. Open symbols correspond to the simulated σ_{iO}-ε_{iO} combinations from the free energy isolines, and filled diamonds correspond to optimized LJ parameters. (b) Free energy profile for the removal of a single water molecule from the first hydration shell as a function of the ion-water oxygen distance for the optimized parameter set.

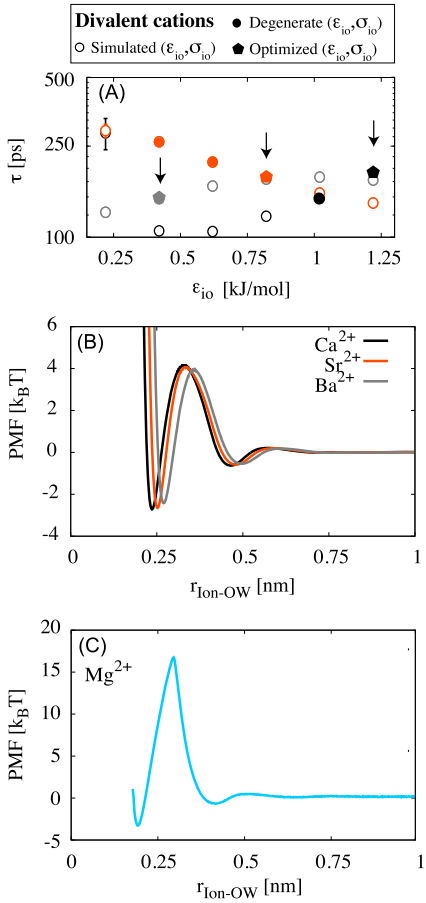

FIG. 8. Water exchange in the first hydration shell of divalent metal cations: (a) Average lifetime of the water molecules in the first hydration shell as a function of ε_{iO} on the free energy isoline for 0.5M salt concentration. Arrows indicate the LJ parameters which capture the characteristic kinetics of water exchange: $(Ca^{2+}) > (Sr^{2+}) > (Ba^{2+})$. Open symbols correspond to the simulated σ_{iO}-ε_{iO} combinations from the free energy isolines. Filled symbols correspond to degenerate parameter combinations (matching experimental solvation free energies and the activity derivatives), and filled diamonds correspond to optimized LJ parameters. (b) Free energy profile for the removal of a single water molecule from the first hydration shell as a function of the ion-water oxygen distance for the optimized parameter set. (c) Free energy profile for Mg^{2+} from umbrella sampling.

ligand exchange experiments:[34] First of all, monovalent ions are more strongly hydrated the higher the charge density as reflected by the increasing depth of the minimum in the PMF. Second, the free energy barrier to remove one water molecule from the first hydration shell increases with increasing ionic charge density. Consequently, the average lifetime is largest for water molecules in the first hydration shell of Li^+ and decreases with decreasing charge density according to $\tau(Li^+) > \tau(Na^+) > \tau(K^+) > \tau(Cs^+)$.

For the divalent cations, the situation is more complex due to the non-monotonic dependence of τ on ε_{iO} for Ca^{2+} [Fig. 8(a)]. This non-monotonic behavior is caused by two opposing trends: Increasing ε_{iO} reduces the free energy barrier as discussed before. At the same time, the hydrated state becomes energetically more and more favorable with increasing ε_{iO}. The non-monotonic behavior allows us to uniquely determine the final parameter set from the degenerated parameter sets for Ca^{2+} and Sr^{2+} since there is only one combination that reflects the experimental trends: $\tau(Ca^{2+}) > \tau(Sr^{2+}) > \tau(Ba^{2+})$. The arrows in Fig. 8(a) indicate the optimal parameter set that simultaneously matches the solvation free energy, the activity derivative, and the characteristic kinetics of water exchange for all divalent metal cations. Figure 8(b) shows the resulting PMF as a function of the ion-water oxygen distance. Ca^{2+} is most strongly hydrated and the free energy barrier associated with water exchange decreases from Ca^{2+} over Sr^{2+} to Ba^{2+} in agreement with experimental results.

What about Mg^{2+}? Compared to the other metal cations, Mg^{2+} is a difficult case since water exchange is much more rare. In fact, direct ^{17}O NMR measurements indicate that the residence time of one water molecule in the first hydration shell is on the order of a microsecond, i.e., 4 orders of magnitude slower compared to Ca^{2+}. Still, first insight can be gained from the PMF as a function of the ion-water distance calculated from umbrella sampling [Fig. 8(c)]. It is evident that the mechanism of water exchange differs significantly from the other ions. First of all, the free energy barrier is much higher and amounts to about 20 k_BT. Second, the free energy profile has a sharp bent in the region of the barrier. Such shapes indicated that the chosen reaction coordinate, namely, the distance between Mg^{2+} and one water molecule, is insufficient to capture the reaction mechanism. A detailed committer analysis shows further that the distance alone is not a good transition state criterion and even fails to correctly assign the basins of attraction (data not shown). In the past, the kinetic rates for water exchange have been estimated based on transition state theory using one-dimensional free energy profiles along the ion-water distance coordinate.[29,50] Unfortunately, since transition state theory relies on an appropriate choice of reaction coordinate, the results are likely to be defective.

Self-diffusion coefficient

In order to gain insight whether the optimized force field parameters correctly describe dynamic quantities, we calculate the self-diffusion coefficient of the ions at infinite dilution. In order to provide accurate results, we take finite size effects and the reduced viscosity of the TIP3P water model into account. The results are listed in Table V together with the experimental results at infinite dilution.[43] For small cations such as Mg^{2+}, Ca^{2+}, and Li^+, the agreement with experiment is quite good, while deviations are observed for larger cations. Still, the agreement between simulations and experiments is much better compared to the computed diffusion coefficients reported in Ref. 53. Note, however, that the simulations by Joung and Cheatham were done at finite salt concentrations and did not take finite size corrections into account. In addition, it is important to consider that TIP3P water diffuses too rapidly. Even though we approximately take this effect into account via Eq. (4), experimental results might be better reproduced in SPC/E and $TIP4P_{EW}$ water. More work is required in order to decide whether the agreement with experimental results could be improved by an advanced treatment of finite size effects in particular the treatment of deviations from the Oseen point-particle limit and the treatment of reduced water viscosity of TIP3P. Otherwise an alternative optimization procedure might be necessary to correctly capture mass transport quantities quantitatively.

CONCLUSIONS

The importance of metal cations for the structure formation, dynamics, and function of biological systems has driven advances in the development of accurate force field parameters for all-atom MD simulations in explicit water over the past years. In order to provide a quantitative description for metal cations, we have developed force field parameters for the biologically most active monovalent and divalent metal cations in conjunction with the TIP3P water model and the Lorentz-Berthelot combination rules. Our optimization procedure is designed to simultaneously reproduce thermodynamic and kinetic properties of aqueous solutions. By systematic optimization, we accurately reproduce the experimental solvation free energy, the activity derivatives, and the characteristics of water exchange from the first hydration shell of metal cations (Tables IV and V). These properties represent a balanced set of solution properties as the basis for a robust model in MD simulations. However, reproducing all experimental properties for metal ions in solutions by the simple and computationally most efficient 12-6 potential turns out to be difficult. Evaluation of the structural properties reveals that it is possible to simultaneously match solvation free energy and coordination number. However, in the parameter range investigated, we observe the limitations in accurately reproducing the ion-water distance as discussed in a number of previous publications.[21,51]

In our parametrization, special emphasis is placed on a proper balance between ion-water and ion-ion interactions, which is essential to quantitatively describe ion specific interactions. This in turn opens up the possibility to resolve the known experimental differences between physiologically very important ions such as Ca^{2+} and Mg^{2+} or Na^+ and K^+ in MD simulations. In our optimization, this is achieved by reproducing the experimental activity derivatives of cation-chloride aqueous solutions. Herein, the standard combination rule for the cation-anion radius for Mg^{2+} has to be modified. This modification has no effect on the transferability, implementation, or

computational speed. Matching experimental activity derivatives allows us to capture the ordering of the ions in terms of a Hofmeister series.[54] This ordering clearly reflects that Mg^{2+} binds its hydration water most strongly. Consequently, Mg^{2+}-water interactions are much stronger than ion-ion interactions. Therefore, Mg^{2+} and Cl^- ions remain solvent separated while larger cations spontaneously from inner-sphere ion pairs. These effects are important to capture ion specific binding to anionic biological groups and ion selectivity of active sites.

In progressing toward improved force fields, it is important to not only capture thermodynamic properties but also capture kinetic properties. In this regard, the parameters of the force field presented here correctly reproduce the characteristics of water exchange from the first hydration shell obtained from ligand exchange experiments. With the exception of Mg^{2+}, the residence time is on the order of a few to a hundred picoseconds and increases with the increasing charge density of the ions (Tables IV and V). Our results show that water exchange is much more rare for Mg^{2+} in agreement with NMR measurements. However, an unambiguous calculation of the residence time using transition state theory and free energy profiles along a simple one-dimensional coordinate is not possible. Here, more work is required in order to derive a meaningful reaction coordinate for a reliable estimate. In the future, it remains to be tested how well parameters optimized for aqueous solutions are transferable to describe the ionic atmosphere around proteins, nucleic acids, and lipids. Yet, with the approach presented, the parameters represent a robust and efficient model to quantitatively capture ion specific binding affinities, ion binding kinetics, and ion competition.

SUPPLEMENTARY MATERIAL

See supplementary material for further discussions of calculated and experimental activity derivatives over a broad concentration range. This material is available free of charge via the Internet at http://pubs.acs.org.

ACKNOWLEDGMENTS

S.M. acknowledges financial support from the Marie Curie IIF 2009 and State S&T program of the Republic of Uzbekistan (BF2-027). N.S. acknowledges financial support from the DFG (Emmy Noether program). Fruitful discussions with D. Horinek are also acknowledged. This research used resources of the National Energy Research Scientific Computing Center, a DOE Office of Science User Facility supported by the Office of Science of the U.S. Department of Energy under Contract No. DE-AC02-05CH11231.

[1] C. F. Anderson and M. T. Record, Annu. Rev. Phys. Chem. **46**, 657 (1995).
[2] R. L. Baldwin, Biophys. J. **71**, 2056 (1996).
[3] B. Alberts, A. Johnson, J. Lewis, M. Raff, K. Roberts, and P. Walter, *Molecular Biology of the Cell* (Garland Science, New York, 2002).
[4] A. M. Pyle, J. Biol. Inorg Chem. **7**, 679 (2002).
[5] K. D. Collins, Methods **34**, 300 (2004).
[6] P. Jungwirth and D. J. Tobias, Chem. Rev. **106**, 1259 (2006).
[7] W. L. Ash, M. R. Zlomislic, E. O. Oloo, and D. P. Tieleman, Biochim. Biophys. Acta **1666**, 158 (2004).
[8] C. Krekeler and L. Delle Site, J. Phys.: Condens. Matter **19**, 192101 (2007).
[9] F. Moucka, I. Nezbeda, and W. Smith, J. Chem. Phys. **139**, 124505 (2013).
[10] Z. Mester and A. Panagiotopoulos, J. Chem. Phys. **142**, 044507 (2015).
[11] Z. Mester and A. Panagiotopoulos, J. Chem. Phys. **143**, 044505 (2015).
[12] A. Benavides, J. Aragones, and C. Vega, J. Chem. Phys. **144**, 124504 (2016).
[13] M. Kohns, S. Reiser, M. Horsch, and H. Hasse, J. Chem. Phys. **144**, 084112 (2016).
[14] M. Kohns, M. Schappals, M. Horsch, and H. Hasse, J. Chem. Eng. Data **61**, 4068 (2016).
[15] I. Nezbeda, F. Moucka, and W. Smith, Mol. Phys. **114**, 1665 (2016).
[16] B. Guillot, J. Mol. Liq. **101**, 219 (2002).
[17] C. Vega and J. L. F. Abascal, Phys. Chem. Chem. Phys. **13**, 19663 (2011).
[18] H. J. C. Berendsen, J. R. Grigera, and T. P. Straatsma, J. Phys. Chem. **91**, 6269 (1987).
[19] W. L. Jorgensen, J. Chandrasekhar, J. D. Madura, R. W. Impey, and M. L. Klein, J. Chem. Phys. **79**, 926 (1983).
[20] S. I. Mamatkulov, M. Fyta, and R. R. Netz, J. Chem. Phys. **138**, 024505 (2013).
[21] D. Horinek, S. I. Mamatkulov, and R. R. Netz, J. Chem. Phys. **130**, 124507 (2009).
[22] I. S. Joung and T. E. Cheatham, J. Phys. Chem. B **112**, 9020 (2008).
[23] J. Åqvist, J. Phys. Chem. **94**, 8021 (1990).
[24] L. X. Dang, J. Am. Chem. Soc. **117**, 6954 (1995).
[25] T. E. Cheatham, M. F. Crowley, T. Fox, and P. A. Kollman, Proc. Natl. Acad. Sci. U. S. A. **94**, 9626 (1997).
[26] P. G. Kusalik and G. N. Patey, J. Chem. Phys. **86**, 5110 (1987).
[27] F. P. Kirkwood and J. G. Buff, J. Chem. Phys. **19**, 774 (1951).
[28] A. P. Lyubartsev and A. Laaksonen, Phys. Rev. E. **55**, 5689 (1997).
[29] M. T. Panteva, G. M. Giambasu, and D. M. York, J. Comput. Chem. **36**, 970 (2015).
[30] M. Fyta, I. Kalcher, L. Vrbka, J. Dzubiella, and R. R. Netz, J. Chem. Phys. **132**, 024911 (2010).
[31] M. Fyta and R. R. Netz, J. Chem. Phys. **136**, 124103 (2012).
[32] P. Li and K. M. Merz, Jr., J. Chem. Theory Comput. **10**, 289 (2014).
[33] I. Yeh and G. Hummer, Biophys. J. **86**, 681 (2004).
[34] L. Helm and A. E. Merbach, Coord. Chem. Rev. **187**, 151 (1999).
[35] S. Kumar, J. M. Rosenberg, D. Bouzida, R. N. Swendsen, and P. A. Kollman, J. Comput. Chem. **16**, 1339 (1995).
[36] I. V. Khavrutskii, J. Dzubiella, and J. A. McCammon, J. Chem. Phys. **128**, 044106 (2008).
[37] G. Hummer, L. Pratt, A. Garcia, B. Berne, and S. Rick, J. Phys. Chem. B **101**, 3017 (1997).
[38] M. R. Reddy and M. L. Berkowitz, Chem. Phys. Lett. **155**, 173 (1989).
[39] T. Darden, D. Pearlman, and L. G. Pedersen, J. Chem. Phys. **109**, 10921 (1998).
[40] G. Hummer, L. Pratt, and A. Garcia, J. Phys. Chem. **100**, 1206 (1996).
[41] G. L. Warren and S. Patel, J. Chem. Phys. **127**, 064509 (2007).
[42] M. D. Tissandier, K. A. Cowen *et al.*, J. Chem. Phys. **102**, 7787 (1998).
[43] Y. Marcus, *Ion Properties* (Marcel Dekker, Inc., New York, Basel, 1997).
[44] L. X. Dang and D. E. Smith, J. Chem. Phys. **99**, 6950 (1993).
[45] S. Weerasinghe and P. E. Smith, J. Chem. Phys. **119**, 11342 (2003).
[46] M. B. Gee *et al.*, J. Chem. Theory Comput. **7**, 1369 (2011).
[47] A. P. Lyubartsev and S. Marcelja, Phys. Rev. E **65**, 041202 (2002).
[48] P. Krüger, S. Schnell, D. Bedeaux, S. Kjelstrup, T. Vlugt, and J. M. Simon, J. Phys. Chem. Lett. **4**, 235 (2013).
[49] S. Schnell, P. Englebienne, J.-M. Simon, P. Krüger, S. Balaji, S. Kjelstrup, D. Bedeaux, A. Bardow, and T. Vlugt, Chem. Phys. Lett. **582**, 154 (2013).
[50] O. Allnér, L. Nilsson, and A. Villa, J. Chem. Theory Comput. **8**, 1493 (2012).
[51] P. Li, B. P. Roberts, D. K. Chakravorty, and K. M. Merz, J. Chem. Theory Comput. **9**, 2733 (2013).
[52] R. A. Robinson and R. H Stokes, *Electrolyte Solutions*, 2nd ed. (Dover, New York, 2002).
[53] I. S. Joung and T. E. Cheatham, J. Phys. Chem. B **113**, 13279 (2009).
[54] F. Hofmeister, Arch. Exp. Pathol. Pharmakol. **24**, 247 (1888).
[55] D. Horinek, A. Herz, L. Vrbka, F. Sedlmeier, S. I. Mamatkulov, and R. R. Netz, Chem. Phys. Lett. **479**, 173 (2009).
[56] J. Wang, W. Wang, P. Kollman, and D. A. Case, J. Mol. Graphics Modell. **25**, 247–260 (2006).
[57] Y. Marcus, Chem. Rev. **88**, 1475 (1988).
[58] F. Jalilehvand, D. Spasgberg, P. Lindqvist-Reis, K. Hermansson, I. Persson, and M. Sandström, J. Am. Chem. Soc. **123**, 431 (2000).
[59] P. R. Smirnov and V. N. Trostin, Russ. J. Gen. Chem. **81**, 282 (2011).